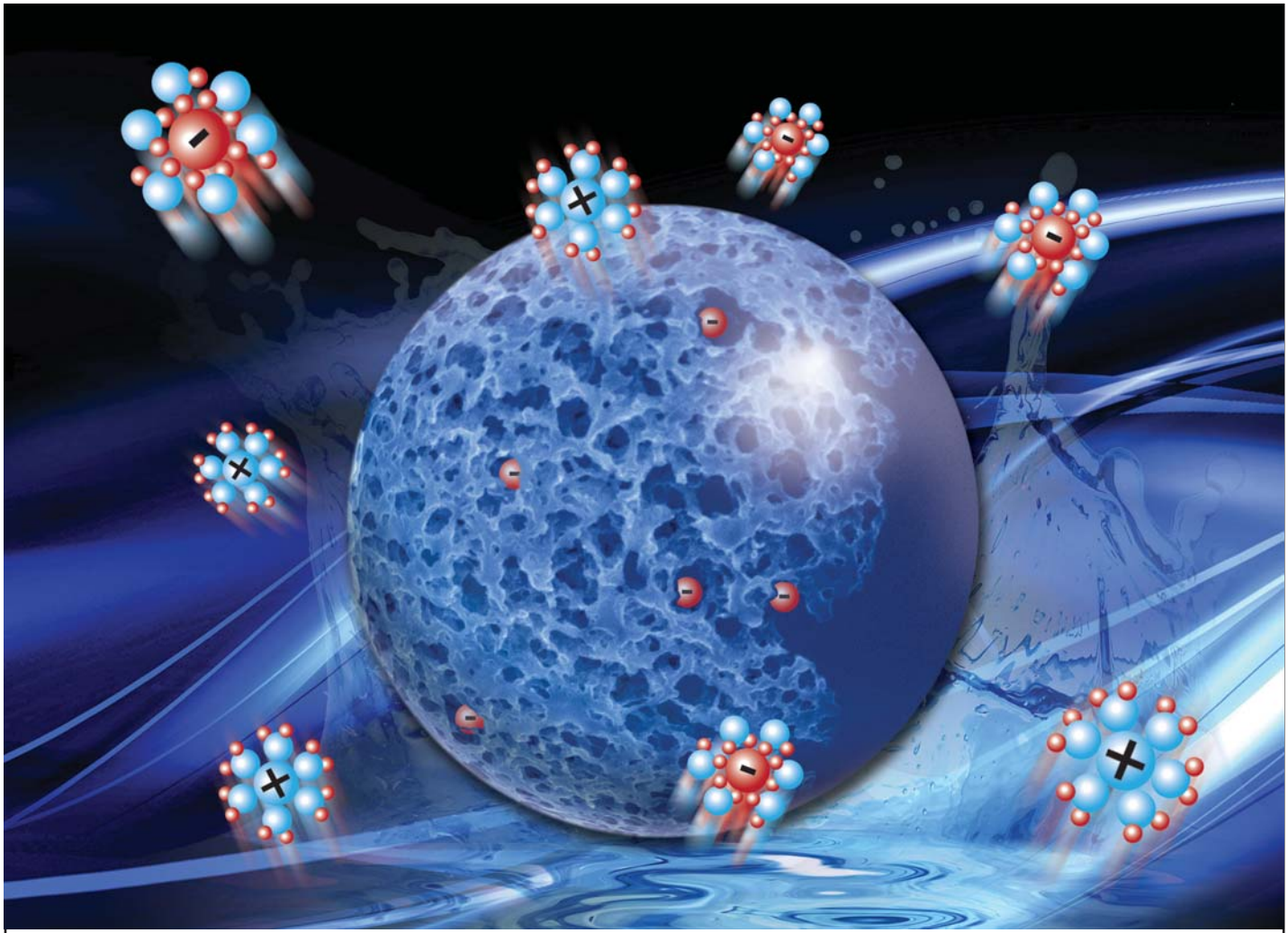

Showcasing research from Lawrence Livermore National Laboratory, California

Title: Advanced carbon aerogels for energy applications

Carbon aerogels hold great technological promise for a variety of sustainable energy applications including hydrogen and electrical energy storage, desalination, and electrocatalysis. Driven by these applications, recent developments in synthetic methodologies have enabled the fabrication of functionalized carbon aerogels with hierarchical morphologies.

As featured in:

See Biener *et al., Energy Environ. Sci.*, 2011, **4**, 656.

RSC Publishing

www.rsc.org/ees

Registered Charity Number 207890

Energy & Environmental Science

Dynamic Article Links

Cite this: *Energy Environ. Sci.*, 2011, **4**, 656

www.rsc.org/ees

PERSPECTIVE

Advanced carbon aerogels for energy applications

Juergen Biener,* Michael Stadermann, Matthew Suss, Marcus A. Worsley, Monika M. Biener, Klint A. Rose and Theodore F. Baumann

Received 3rd November 2010, Accepted 4th February 2011
DOI: 10.1039/c0ee00627k

Carbon aerogels are a unique class of high-surface-area materials derived by sol–gel chemistry. Their high mass-specific surface area and electrical conductivity, environmental compatibility and chemical inertness make them very promising materials for many energy related applications, specifically in view of recent developments in controlling their morphology. In this perspective we will review the synthesis of monolithic resorcinol–formaldehyde based carbon aerogels with hierarchical porosities for energy applications, including carbon nanotube and graphene composite carbon aerogels, as well as their functionalization by surface engineering. Applications that we will discuss include hydrogen and electrical energy storage, desalination and catalysis.

1. Introduction

The expression "the new carbon age" has been coined to express the rapid development of carbon-based nanomaterials that hold great technological promise for a variety of applications. Well-known examples are zero-dimensional buckyballs, one-dimensional carbon nanotubes (CNTs) and the relatively new class of two-dimensional graphene nanosheets, the subject of the 2010 Nobel Prize in Physics. Another equally important class of carbon nanomaterials are the three-dimensional nanoporous carbons, the development of which holds great technological promise for a variety of sustainable energy applications, including energy storage, adsorption and catalysis.[2–7] All these new carbon nanomaterials have in common that they are built from sp^2-hybridized 'graphitic' carbon atoms, thus providing them with mechanical strength and unique electronic properties.

Physical and Life Science Directorate, Lawrence Livermore National Laboratory, 7000 East Avenue, California, 94550, USA. E-mail: biener2@LLNL.gov

The utility of porous carbons is derived from their high surface area, three-dimensional structure, chemical stability, the abundance of carbon, and their low mass density.[8] Among these, carbon aerogels (CAs) are specifically promising in that they possess a *tunable three-dimensional hierarchical* morphology with ultrafine cell sizes and an electrically conductive framework, and that they are available as macroscopic, centimetre-sized monolithic materials.

Aerogels in general are a special class of open-cell foams that exhibit many fascinating properties, such as low mass densities, continuous porosities and high surface areas. These unique properties are derived from the aerogel microstructure, which typically consists of three-dimensional networks of interconnected nanometre-sized primary particles. Aerogels are typically prepared using sol–gel chemistry, a process that involves the transformation of molecular precursors into highly cross-linked inorganic or organic gels that can then be dried using special techniques (*i.e.* supercritical drying, freeze drying, *etc.*) to preserve the tenuous solid network. For organic and carbon aerogels, this transformation involves the polymerization

Broader context

Reducing our dependence on fossil fuels and moving towards renewable energies will be a crucial step towards a sustainable future. Hydrogen generated from water by solar energy and electric energy from sustainable resources are widely considered as fuels of the future. The efficiency of many of the new technologies that will come with a sustainable energy economy will depend on the availability of new functional nanomaterials. Here, porous carbons are one class of materials that can be expected to play a key role due to their unique combination of properties such as high surface area, electrical conductivity, chemical stability, and environmental compatibility. Among these porous carbons, carbon aerogels (CAs) are specifically promising in that they possess a *tunable* three-dimensional hierarchical morphology, and that they are available as macroscopic monolithic materials. This perspective provides an overview of recent progress in synthetic methodologies for CA fabrication, and discusses the morphological and functional diversity of CAs in the context of the requirements for some of their most promising applications, including hydrogen and electrical energy storage, desalination, and catalysis.

of multi-functional organic species into three-dimensional polymer networks. Although the first aerogels based on silica gels were discovered already in 1931,[9] it took another 60 years until polymer-based carbon aerogels were developed by Pekala *et al.*[10,11] in the late eighties at Lawrence Livermore National Laboratory. Their potential as electrode materials, however, was immediately recognized.[12] These materials are prepared through simple sol–gel polymerization of organic precursors, such as resorcinol and formaldehyde, in aqueous solution and thus are mass producible. The sol–gel process yields highly cross-linked organic gels that then are supercritically dried and subsequently pyrolyzed in an inert atmosphere.[10] The pyrolysis transforms the organic aerogel precursor into a porous carbon network comprised of both amorphous and graphitic (turbostratic microcrystalline) regions. The graphitic domains within CAs, however, are typically quite small and contain a significant amount of disorder. Unlike many other porous carbon materials, CAs can be fabricated in a variety of forms, including monoliths and thin films, a feature that can be advantageous for many applications. Furthermore, the synthesis of CAs can be easily adjusted to produce materials with very different three-dimensional architectures (see Fig. 1) which allows one to tailor the transport properties of CAs. Because of their unusual chemical and textural characteristics, carbon aerogels are promising materials for use as electrode materials in supercapacitors and rechargeable batteries, advanced catalyst supports, adsorbents, and thermal insulation.[1,13–20] This article provides an overview of recent progress in synthetic methodologies, and discusses the morphological and functional diversity of CAs in the context of the requirements for some of their most promising applications in the field of hydrogen storage, electrical energy storage, desalination, and catalysis.

2. Design of carbon aerogels

The technological promise of CAs comes from the fact that their morphology, and thus their properties can be controlled by the sol–gel reaction chemistry. Several factors of the polymerization reaction have a significant impact on network formation in these materials (Fig. 1). The choice of sol–gel precursors, polymerization catalyst and reaction solvent can be used to control the structure of the resultant gel. As an example, the amount and type of polymerization catalyst used in the sol–gel reaction influence the nucleation, growth and interconnectivity of the primary particles that comprise the aerogel framework.[21] Formulations that utilize low catalyst concentrations typically produce gels with larger primary particles as compared to those generated from higher catalyst concentrations. The morphology and spatial arrangement of these particles, in turn, determine the bulk physical properties of the CA. For instance, electrical conductivity in CAs occurs through the movement of charge carriers through individual carbon particles and "hopping" of these carriers between adjacent carbon particles.[22] Therefore, charge transport is highly dependent on interconnectivity of the carbon network. Likewise, a number of other bulk properties, such as specific surface area, average pore size, compressive modulus and thermal conductivity, correlate with the network architecture and, therefore, can be tuned through the reaction chemistry.

To further optimize the properties of CAs for specific applications, recent efforts have been focused on the functionalization of the CA framework, either through modification of the aerogel surface or through incorporation of additives, such as catalyst nanoparticles or carbon nanotubes, into the framework structure. The flexibility of the CA synthesis readily allows for systematic modification of the extended network structure (Fig. 1). For example, functionalized sol–gel precursors can be used in the polymerization reaction to introduce a specific functional group into the organic and carbon aerogel framework.[23–27] This approach has been used to homogeneously incorporate metal nanoparticles into CA matrices. Another approach to modify the CA framework involves the integration of additives, such as carbon nanotubes or graphene sheets, into the sol–gel reaction.[28–34] Sol–gel polymerization of the precursors in the presence of the additives leads to the formation of composite structures in which the additive becomes a part of the primary carbon network structure. This approach can be used to enhance the electrical, thermal and mechanical properties of the composite material relative to the pure CA as recently demonstrated for CNT additives.[29] Templates can also be used in the sol–gel polymerization reaction to impart specific structural features to the porous solid under construction.[35–39] After gel formation, these templates can be removed, either chemically or thermally, to yield an ordered network of pores within the aerogel framework. Using this technique, materials with bimodal pore structures can be prepared in which the large ordered cavities formed by the template are continuous and interconnected, while smaller meso- and microporous channels run continuously throughout the aerogel wall. Hierarchically porous structures of this type present a number of advantages over unimodal carbon structures in terms of diffusion efficiency and surface area, and thus these materials have utility as catalyst supports or electrodes for electrochemical devices.

Alternatively, the surfaces of the aerogel framework can also be modified after the carbonization step through gas- or solution-phase reactions within the open pore volume of the aerogel. Typically, these structures are sufficiently robust to withstand the

Marcus A. Worsley, Theodore F. Bauman, Matt Suss, Michael Stadermann, Monika M. Biener and Juergen Biener

From left to right: Marcus A. Worsley and Theodore F. Bauman from the Advanced Materials Synthesis group, Matt Suss from the Engineering Division, Michael Stadermann from Chemical Sciences Division, and Monika M. Biener and Juergen Biener from the Nanoscale Integration Science & Technology Group at LLNL. Not shown: Klint A. Rose from the Engineering Division. Together they share an interest in the physics of nanostructured high surface area materials, and applying their unique properties to energy related technologies. They have published more than 190 papers in the field of nanoscale materials and surface related phenomena.

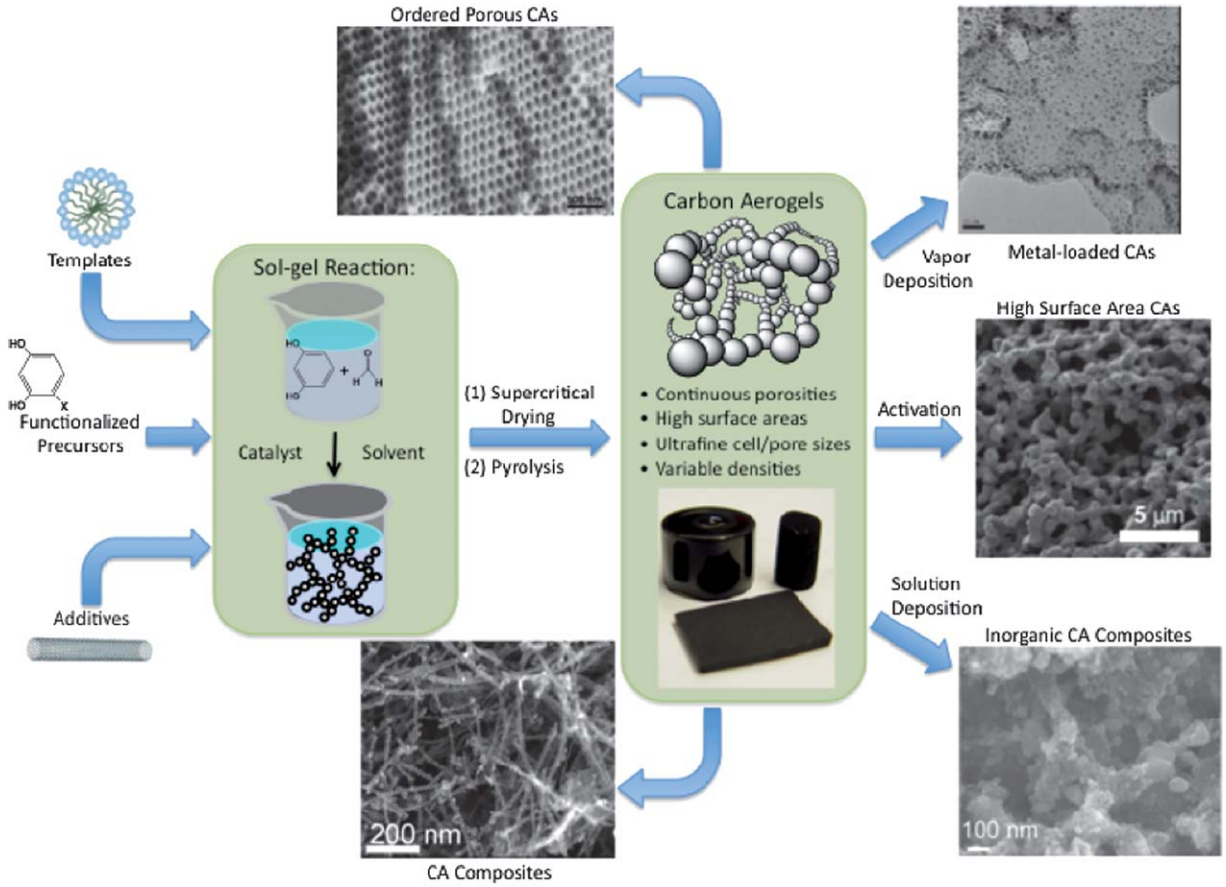

Fig. 1 Synthetic scheme showing the versatility associated with carbon aerogel synthesis. As shown, the CA structure can be modified either during the sol–gel polymerization step, through the introduction of additives or templates to the reaction mixture, or through gas- or solution-phase reactions on the surfaces of the CA framework after the pyrolysis step.

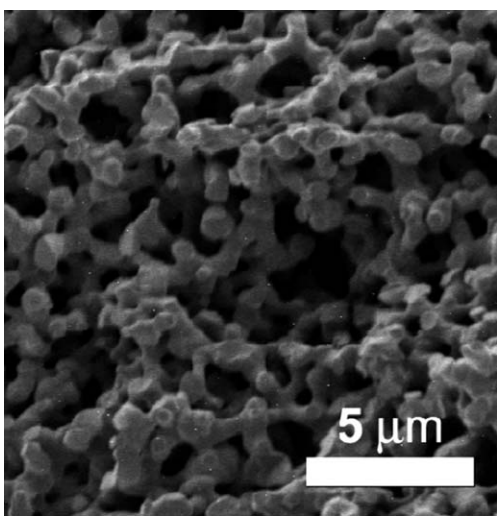

Fig. 2 SEM image of an activated CA with a surface area of ~3100 $m^2\ g^{-1}$.

compressive forces associated with re-wetting and drying of the material. These modifications can range from thermal activation[40–44] to electrochemical deposition of a secondary material directly on the surface of the carbon framework.[45–48] For example, the thermal activation process has been used to prepare CAs with Brunauer–Emmett–Teller (BET) surfaces in excess of 3000 $m^2\ g^{-1}$ (total pore volume ≈ 4.5 $cm^3\ g^{-1}$) that have been investigated as gas sorbents and electrodes.[40] Self-limiting electroless deposition processes have been used to "paint" the interior structure of CA materials with electroactive species, such as MnO_2, for the design of new capacitors.[45–48] Inorganic CA composites have also been prepared through the sol–gel polymerization of inorganic species on the internal surfaces of monolithic CA parts.[49–51] With this approach, the inorganic species (metal oxides such as SiO_2, TiO_2 or ZnO) form a conformal overlayer on the primary ligament structure of the CA. Nanocomposites formed from carbon and these metal oxides have the potential to exhibit enhanced functional properties for catalysis and energy storage applications. As described in Section 3.4, gas phase deposition techniques, such as atomic layer deposition, are another extremely powerful approach to deposit inorganic species, such as catalyst nanoparticles or insulating overlayers, on the inner surfaces of CA substrates.[1,52,53] This approach has even been extended to the use of CAs as substrates for the direct growth of carbon nanotubes by chemical vapor deposition.[54] By engineering the pore structure of the CA substrate, uniform CNT yield can be achieved throughout the free internal pore volume of CA monoliths with macroscopic dimensions. Clearly, the flexibility associated with

CA synthesis provides tremendous opportunity for the design of new nanostructured materials for energy related applications.

3. Applications

The hierarchical 3D morphology of CAs and the fact that structural parameters, such as surface area and pore size distributions, can be controlled systematically make CAs attractive materials for applications that require both high surface areas and fast mass transport. The most promising emerging applications of CAs in this field are hydrogen storage, electrical energy storage using the electric double layer capacitor technology, desalination using the capacitive deionization technique, and their use as catalytic supports in, for example, fuel cells. The performance of CAs in these applications strongly depends on their three-dimensional architecture. For example, the storage capacity of CAs for both hydrogen and electrical energy depends on the presence of micropores to provide surface area, whereas the dynamics of loading and unloading depends on the presence of macropores to facilitate mass transport. In the following sections we will discuss some of the most promising energy-related applications of CAs with an emphasis on functional requirements.

3.1 Hydrogen storage

One area of carbon research that has received significant attention is the use of porous carbon materials as sorbents for hydrogen.[55–59] Safe and efficient storage of hydrogen is considered one of the main challenges associated with utilization of this fuel source in the transportation sector.[60] Two important criteria required for effective hydrogen physisorption are (1) a high surface area that exposes a large number of sorption sites to ad-atom or ad-molecule interaction[61] and (2) sufficiently deep potential wells so that the storage material can be utilized at reasonable operating temperatures. Porous carbons are promising candidates for hydrogen physisorption due to their lightweight frameworks and high accessible surface areas. The low hydrogen binding energies, however, that are typical of carbonaceous sorbents (~6 kJ mol^{-1} H_2), require that cryogenic temperatures (77 K) be utilized for storage of hydrogen in these materials. In general, the amount of surface excess hydrogen adsorbed on porous carbons at 77 K and ~3.5 MPa varies linearly with BET surface area, and the gravimetric uptake is ~1 wt% H_2 per 500 m^2 g^{-1} of surface area.[59,62]

A new class of ultra-high surface area CAs was recently developed for use as hydrogen physisorbents.[20,40] These materials were prepared through thermal activation, a process that involves the controlled burn-off of carbon from the aerogel structure in an oxidizing atmosphere, such as carbon dioxide. Carbon removal creates new micropores (pores smaller than 2 nm) in the structure and, therefore, increases the overall surface area of the aerogel. Using this approach, new CA sorbents with BET surface areas in excess of 3000 m^2 g^{-1} were prepared (Fig. 2). These values are greater than the surface area of a single graphene sheet (2630 m^2 g^{-1}, if both graphene surfaces are taken into account). Presumably, edge termination sites constitute a substantial fraction of the surface area in these activated CAs, as is the case for traditional high surface area activated carbons. Hydrogen uptake at 77 K in the activated CAs scaled linearly with the BET surface area up to 2500 m^2 g^{-1}, yielding gravimetric densities up to 5 wt% H_2 (Fig. 3), comparable to the highest values measured in porous carbons.[59] Above 2500 m^2 g^{-1}, the differential increase in the hydrogen storage capacity is smaller than expected, likely due to increase in the pore size in this ultrahigh surface area material. Previous studies have shown that size and shape of the pores in hydrogen physisorbents play a critical role in hydrogen uptake, with the optimal structure having slit-shaped pores with diameters between 0.7 and 1 nm.[63,64] As shown in Fig. 4, increasing activation does not only increase the surface area of the sorbent, but also shifts the pore size distribution to larger values. In addition to gravimetric capacity, volumetric capacity is an equally important consideration in the design of functional hydrogen sorbents. Depending on the density of the CA, the volumetric capacity of these materials can range from 10 to 29 g H_2 L^{-1}. While these values are on par with those of other porous carbon materials, further optimization of CA pore structure is required for increased hydrogen energy density.

The hydrogen binding enthalpies measured for the activated CAs were ~6 kJ mol^{-1}, as would be expected for a carbon-based sorbent. As mentioned above, the low binding energies associated with porous carbons are an obstacle to meeting capacity requirements at reasonable operating temperatures (>273 K). Previous work has shown that hydrogen adsorption energies near 15 kJ mol^{-1}, over the full range of surface coverage, are necessary to meet this requirement.[65] Numerous approaches have thus been employed to improve the thermodynamics of hydrogen binding in porous carbons while retaining large surface areas for sorption. The hydrogen spillover effect, for example, has been suggested as a mechanism to increase the reversible hydrogen storage capacity at room temperature in metal-loaded carbon nanostructures.[66–69] The spillover process involves the dissociative chemisorption of molecular hydrogen on a supported metal

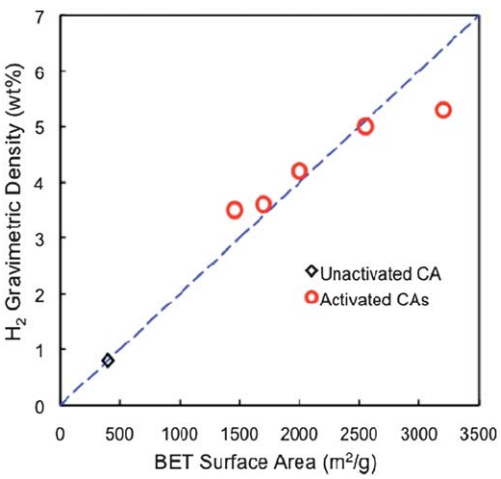

Fig. 3 Excess gravimetric density (wt% H_2) saturation value at 77 K as a function of BET surface area for the activated CAs. The dotted line shows the correlation of 1 wt% H_2 per 500 m^2 g^{-1}. It is important to note that surface excess hydrogen values are a measure of H_2 adsorbed *on* the surface of the CA only and do not account for free hydrogen gas in the pores of the CA. Therefore, total gravimetric hydrogen capacities in these CA materials are higher than the surface excess values.

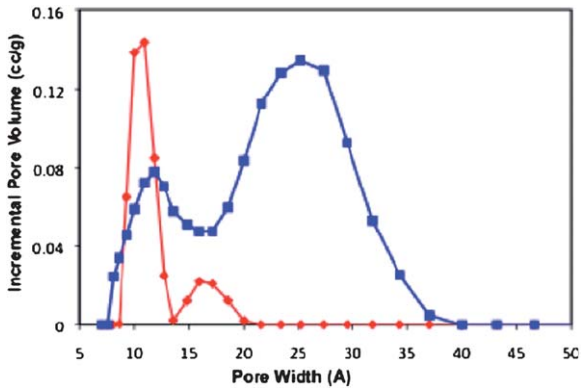

Fig. 4 Pore size distribution for activated CAs with BET surface areas of 1500 (red) and 3100 (blue) $m^2\ g^{-1}$, as determined from the N_2 adsorption isotherm using the density functional theory (DFT) method.

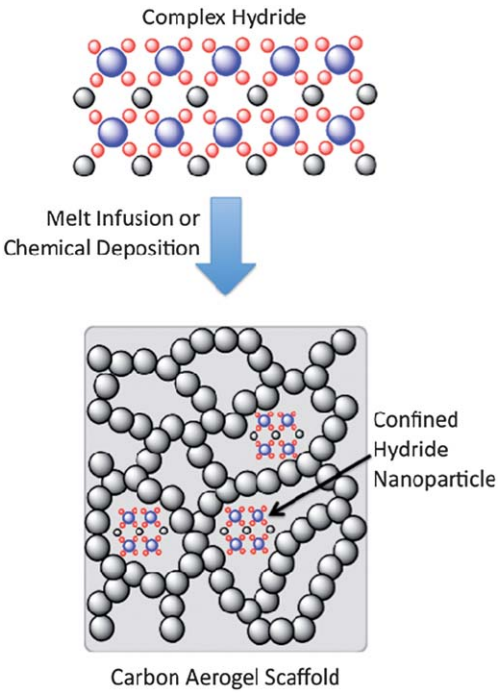

Fig. 5 The scaffolding approach involves the confinement of nanostructured hydride material within the free pore volume of a nanoporous scaffold material, such as a carbon aerogel.

catalyst surface (*e.g.* platinum or nickel), followed by the diffusion of atomic hydrogen onto the surface of the carbon support. Alternatively, substitutional doping of carbon with boron or other light elements has also been presented as a promising route toward increasing hydrogen binding energy in these sorbent materials.[70,71] The flexibility associated with CA synthesis allows for the incorporation of such modifiers into the carbon framework. For example, gas- and solution-phase deposition techniques have been developed that allow for uniform incorporation of metal nanoparticles into the carbon framework (see also the Catalysis section). The performance of these modified CAs as next generation hydrogen storage materials is currently being evaluated.

Beyond their use as hydrogen sorbents, CAs have also been used to enhance the performance of other solid-state hydrogen storage materials, specifically complex hydrides, such as alanates (AlH_4^-), amides (*i.e.* NH_2^-) and borohydrides (BH_4^-). Complex hydrides offer a number of advantages for the storage of hydrogen, including high gravimetric and volumetric hydrogen capacities.[72,73] The thermodynamics and kinetics associated with reversible hydrogen storage in these systems, however, present significant obstacles to their utilization as storage materials at reasonable operating temperatures and pressures. Incorporation of complex hydrides into the free pore volume of a nanoporous solid or scaffold has been shown to improve the rates of both hydrogenation and dehydrogenation for these materials (Fig. 5). The enhanced kinetics can be attributed to the shorter diffusion distances for hydrogen as well as the other elements (*i.e.* Li, B, *etc.*) in the nanostructured hydride. Practical application of the scaffold approach requires the design of porous solids with small pore sizes to physically confine the nanostructured hydride as well as large accessible pore volumes to minimize the gravimetric and volumetric capacity penalties associated with the use of the scaffold in a storage system. In addition, these scaffold materials should be chemically inert, mechanically robust and capable of managing thermal changes associated with the cycling of the incorporated hydride. While a variety of porous matrices have been investigated as scaffolds,[74–78] CAs have emerged as one of the most promising candidates due to their large pore volumes and tunable porosities, as well as for the ability to modify the surface characteristics of the carbon framework. As described above, the pore structure of CAs can be controlled through the sol–gel polymerization conditions (*i.e.* R/C ratio, concentration of reactants), allowing for the fabrication of monolithic scaffolds with large internal pore volumes distributed over nanometre-sized pores. Recent work by several groups has demonstrated the promise of the CA scaffolding approach with a number of different hydrogen storage materials. For example, incorporation of $LiBH_4$ into CA scaffolds was shown to significantly enhance the rate of hydrogen exchange in the material relative to that of bulk $LiBH_4$, and that the effect is inversely correlated with the average pore size of the scaffold (*i.e.* smaller pores yielding faster kinetics).[17] In fact, the rate of dehydrogenation for $LiBH_4$ was shown to increase by as much as 50 times at 300 °C in a CA with 13 nm pores. Similar improvements in dehydrogenation kinetics were also reported for $NaAlH_4$ incorporated into a small pore CA scaffold.[79,80] In addition, the $NaAlH_4$ within the scaffold, unlike bulk $NaAlH_4$, could be readily rehydrogenated to full capacity at ~160 °C under 100 bar H_2. The desorption kinetics of other solid-state hydrogen storage materials, such as MgH_2 and NH_3BH_3, were also affected considerably when embedded within the pores of a CA scaffold.[81–85] Despite these promising results, additional efforts in this area are necessary to better understand the influence of the CA textural properties and surface chemistry on the performance of the incorporated hydride. Further optimization of the aerogel architecture is also required for the design of robust scaffolds that can accommodate larger weight fractions of the complex hydride. These structural refinements present a challenging trade-off in terms of porosity and mechanical properties. Increasing the pore volume in these scaffolds while maintaining small pore sizes requires that the walls defining the pore structure be very thin. The thickness of

the wall structure, in turn, determines the mechanical integrity of the material. This aspect of scaffold design is an important consideration, as these materials need to have sufficient mechanical strength to withstand the stresses associated with infiltration and cycling of the hydride. Nevertheless, CA scaffolds represent a promising option for improving the performance of metal and chemical hydride systems.

3.2 Supercapacitors and batteries

The storage of electrical energy is one of the important hurdles that needs to be overcome for the widespread implementation of many "green" technologies, and the most common application of CAs in this field is the electrical double-layer capacitor (EDLC).[86] In these devices, charge is stored in the form of ions accumulated on the surface of the material (Fig. 6), thus creating an intermediate between batteries and electrostatic capacitors.[87] The energy density is lower than that of a battery, but higher than that of an electrostatic capacitor. The inverse is true for power density. The high rate capability and cyclability make the EDLC an ideal complement to batteries in devices with peak power demands significantly above the base level, where they extend the life of the battery. A typical example is the use of supercapacitors for regenerative braking in electric and hybrid cars. However, the high cost of the EDLCs, as well as their limited energy density, has so far prevented them from replacing batteries more widely.[88]

Focus areas of EDLC development include (1) increasing of energy and power densities, (2) increasing the operating voltage and (3) decreasing the cost per Wh stored in the device. Improving these properties requires the development of advanced electrode materials, and CAs are ideally suited for this purpose as they are chemically inert, highly conductive, environmentally friendly, can be made from cheap and abundant raw materials, and most importantly, provide high specific surface areas combined with a fully tunable 3D structure. Specifically the tunability of the CA structure provides a tool for improving energy and power densities, as both depend on the pore structure of the electrode. Very promising is the development of hierarchically structured CAs containing both macropores to facilitate mass transport and provide power density, and micro/mesopores to provide the required high surface area for energy density. The area-specific capacity of the electrode material is of critical importance for the performance of an EDLC. Thus much effort has been devoted in recent years to increase the area-specific capacity by pore-size engineering. The two important observations that have been made are: (1). the area specific capacitance decreases with decreasing pore size[89] as the access of solvated ions gets more and more sterically hindered and part of the surface can no longer be utilized, and (2) once the pores become smaller than the hydrated ion radius, the specific capacitance increases again due to the distortion and reduction in size of the ion solvation sheath in sub-nm pores.[4] The pore size also affects power density: if the pore contains fewer ions than necessary to charge the pore, then ions must diffuse through the electrode to fully charge the device, resulting in lower charge/discharge rates.[90] Additionally, pore size, tortuosity, length and shape of the pores all affect the resistance of the capacitor and thus its power density. It is expected that exploiting the tunability of the CA structure will lead to CA electrodes with greatly improved performances.

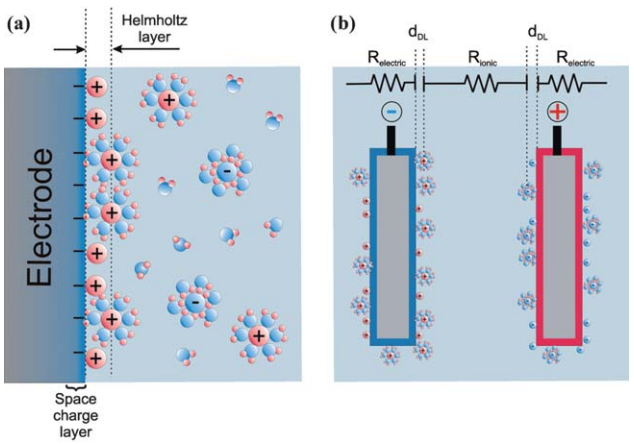

Fig. 6 (a) Electric double layer (EDL) model showing the accumulation of cations at a negatively polarized electrode surface in contact with an electrolyte. In the case of an ideally polarizable electrode, no charge transfer takes place across the electrode/electrolyte interface, leading to a capacitor-like separation of positive and negative charges. The atomic-scale dimensions of the EDL result in much higher capacities compared to those of a conventional parallel-plate capacitor. (b) An EDLC consists of two EDL capacities in series (one at each electrode). The electrode needs to be chemically inert, exhibit a high surface area, and allow for fast diffusional mass and electronic transport.

Hierarchically structured CAs are ideally polarizable high capacitance electrodes as demonstrated by the box-shaped cyclic voltammetry (CV) curve shown in Fig. 7. The CA in this example has a specific capacitance of $\sim$100 F g^{-1}. Increasing the potential window, however, leads to undesirable Faradaic losses due to the onset of water breakdown and/or carbon corrosion. Hierarchically structured CA electrode materials have also the potential to considerably improve the dynamic performance of EDLCs. Hierarchically structured CAs charge faster and with less resistive losses as indicated by both the larger rise in capacitance and lower resistance with decreasing frequency (Fig. 8).

When it comes to improving the energy density of carbon-based electrodes, the question is what is the physical limit of the area specific capacitance? Literature values of the specific capacitance for carbon range from $\sim$3 μF cm^{-2} for graphitic carbon[91] to $\sim$50 μF cm^{-2}.[92] Thus, an activated CA with a surface area of $\sim$3000 m^2 g^{-1} could theoretically exhibit gravimetric specific capacitance values as high as 1500 F g^{-1}. However, experimentally observed values are much lower than those predicted by this simple linear extrapolation. For example, our experimental values for the gravimetric specific capacitance obtained from various CA samples with different morphologies, densities and compositions increase with increasing surface area from $\sim$50 F g^{-1} for a 600 m^2 g^{-1} material to only $\sim$110 F g^{-1} for a $\sim$3000 m^2 g^{-1} CA (Fig. 9). Obviously, most of the 5-fold increase in surface area is compensated by a decreasing area specific capacitance that decreases from $\sim$8 μF cm^{-2} for the 600 m^2 g^{-1} material to $\sim$3 μF cm^{-2} for the 3000 m^2 g^{-1} CA. Several explanations can be brought forward: (1) with increasing surface area an increasing fraction of the pores is smaller than the radius of hydrated ions, and thus no longer accessible. Thus pore

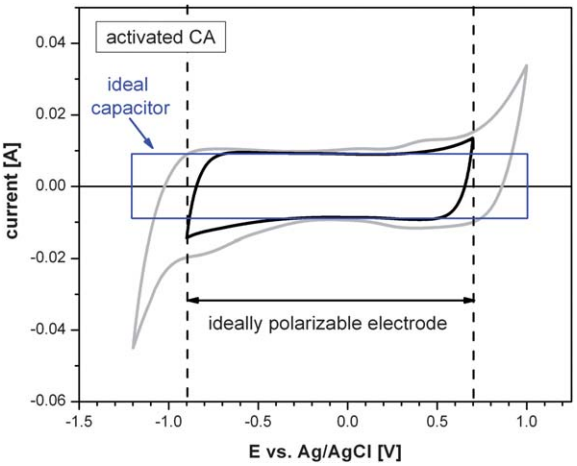

Fig. 7 Cyclic voltammetry (CV) data collected from a hierarchically structured high-surface-area CA electrode (~2400 $m^2 g^{-1}$, three electrode setup in 1 M NaCl). The box-shaped CV within the potential range from −0.9 to 0.7 V (*vs.* Ag/AgCl) is characteristic for an ideally polarizable electrode, whereas the increasing current at higher potentials indicates undesirable Faradaic losses due to the onset of water breakdown and/or carbon corrosion.

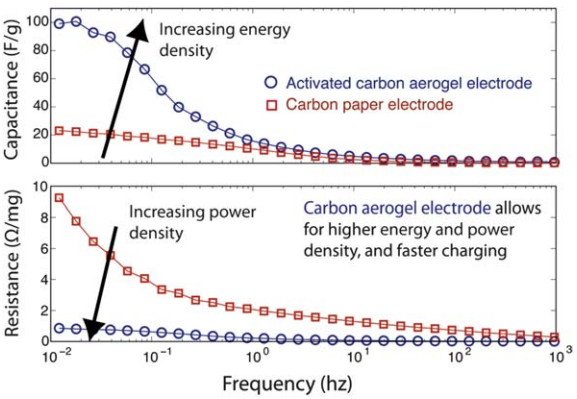

Fig. 8 Frequency dependent capacitance and resistance of porous carbon electrodes in 0.5 M NaCl, from electrochemical impedance spectroscopy (EIS) data (collected at 0.1 V *vs.* Ag/AgCl, 20 mV amplitude). Compared to carbon paper, the hierarchically structured activated CA charges faster and with less resistive losses.

size engineering should allow creating materials with much higher capacities; (2) the capacitance may be controlled by the solid side, where the small density of states at the Fermi level in graphite-like carbon implies small capacitance, in which case only band structure engineering would allow obtaining higher values; and (3) experimental reference values obtained from low-surface-area materials such as bulk graphite samples overestimate the area specific capacity as the calculation of these values is typically based on a geometric surface area rather than the unknown real surface area.

This discussion makes clear that the surface functionality may play an important role, and that synthesis conditions can make an important difference to the final capacitance of the device. Indeed, post-treatment of the surface, through oxidation of the carbon or coating with other materials, such as conducting

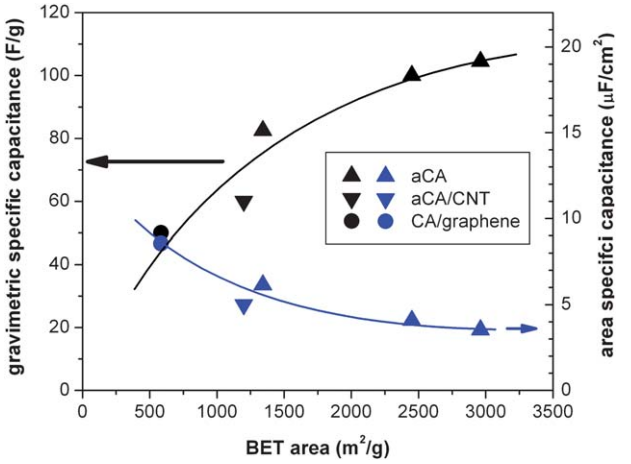

Fig. 9 Gravimetric and area specific capacitance *versus* surface area for activated CAs (▲) as well as activated CA/carbon nanotube (▼) and CA/graphene (●) composite materials. The gravimetric specific capacitance increases and the area specific capacitance decreases with increasing surface area.

polymers or transition metal oxides, has been shown to increase the specific capacitance four- to ten-fold, usually at the cost of reducing the surface area.[93] The depositions can be performed electrochemically, through gas phase deposition (*e.g.* atomic layer deposition) or through wet chemistry. While it is possible to prepare electrodes made entirely out of transition metal oxides,[48] it may still be advantageous to use a CA as a backbone to utilize the good control over morphology and the high intrinsic conductance that the CA provides.

Instead of increasing the specific capacitance, one could also utilize surface functionalization to increase the operating voltage by coating the CA electrode surface with a high dielectric constant material such as alumina or titania. This creates an electrolytic capacitor-like device that can be operated at voltages up to the breakdown voltage of the dielectric, rather than that of the electrolyte. The energy density change produced by coating the electrode with a dielectric layer will be strongly affected by the structure of the aerogel: the energy of a capacitor scales with 0.5 CV^2 where C is the capacitance and V is the applied voltage. The breakdown voltage of the dielectric layer scales linearly with the layer thickness d. The capacitance, on the other side, scales with $1/d$ and is proportional to the surface area. To achieve a net gain, the loss of surface area caused by the coating must be smaller than the gain from the increased breakdown voltage and dielectric constant. Micropores would be covered or filled in by even thin coatings, and thus the energy density of these structures is likely to decrease. Meso- and macroporous materials, on the other hand, will not see significant losses in surface area until larger values for d are reached, and thus should benefit from dielectric coatings. Even if there is no net gain in volumetric or gravimetric capacitance, the devices with higher operating voltage will outperform the unfunctionalized devices in high-voltage applications: to reach the higher operating voltages typical for EDLC applications, one has to stack n of them in series, which causes the capacitance to drop as $1/n$, in which case the device with the higher operating voltage would perform better even if its gravimetric capacitance is lower.

For very high voltages, aerogel-based electrolytic capacitors are not likely to exceed the performance of conventional electrolytic capacitors, but in the 10 V range, the control over aerogel morphology may be able to produce a superior device.

One major drawback of CAs for the EDLC application is their low density (<500 mg cm^{-3}) that limits the achievable volumetric energy density. One strategy to increase the performance of CA electrodes for the EDLC application in terms of energy density is to increase their volumetric surface area and capacitance (m^2 cm^{-3} and F cm^{-3}). This can be achieved by filling a fraction of the open porosity of the CA with another high-surface-area material, for example by chemical vapor deposition of carbon nanotubes.[54]

CAs may also find future use in batteries, either as current collectors with tunable porosities[94] or scaffolds for 3D intercalated batteries.[95] In the first function, they provide the same advantages for the power of the device as they do in capacitors: the tunable porosities can be used to minimize diffusion resistance while maintaining a constant surface area, thus reducing internal resistance as well as polarization potentials and increasing the power density of the device. At the same time, the aerogel can function as a low density current collector that is directly functionalized and eliminates the need for binder and filler, which increases the energy density. Finally, the CA scaffold provides a means to utilize lithium intercalation materials usually limited by large volumetric changes, such as Sn or Si, which would be coated onto the current collector in very thin layers and thus subjected to lower stresses.[96,97] In the second function, the control over morphology can again be used to create a structure that facilitates the assembly of the intercalated battery, and the previously listed coating and functionalization methods can be brought to bear to perform the actual assembly of the battery.

3.3 Capacitive deionization

Freshwater is one of earth's most valuable resources, and many regions suffer from an increasingly limited freshwater supply. Consequently, boosting supply through desalination of seawater and brackish water from saline aquifers, which together account for over 97% of all water, is increasingly important.[98]

CAs have considerable potential to significantly improve desalination efficiency through a technique known as capacitive deionization (CDI). Like the supercapacitor, CDI relies on the formation of an EDL to store charge (Section 3.3, Fig. 6). In CDI, however, the goal of the charge storage is not energy storage, but charge removal from the electrolyte: the electrolyte is seawater or brackish water *flowing* between the electrode pairs, and the charging of the electrodes and formation of the double layer significantly *deplete* the ion concentration in the electrolyte (Fig. 10). CDI has potentially significant advantages over other, more conventional, water desalination techniques such as reverse osmosis (RO) that is currently the fastest growing desalination technique.[98,99] RO is an energy- and infrastructure-intensive process, because it relies on forcing sea or brackish water through a membrane with low salt permeability by applying a pressure several times that of the osmotic pressure (typically 1–10 MPa),[99] and because it requires pressure exchangers or turbines to recover some of that energy.[99] The advantages of CDI over RO are that: (1) it requires no membrane elements, (2) it can desalinate water at low (sub-osmotic) pressures, and (3) energy can be

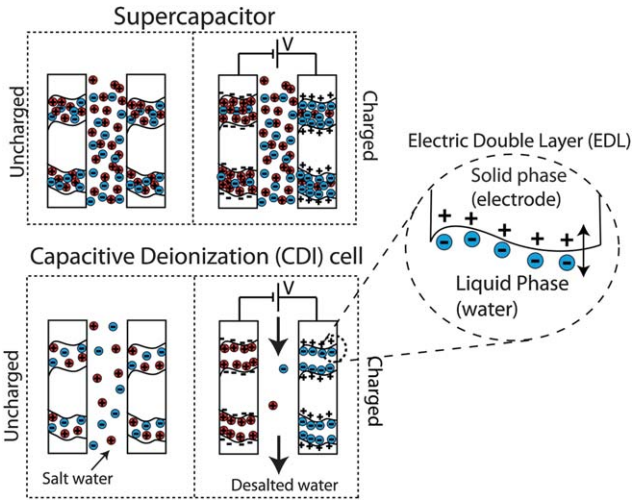

Fig. 10 Schematic representation of the differences between a supercapacitor cell for energy storage (top) and a CDI cell for brackish water desalination (bottom). Both systems consist of two porous electrodes separated by an electrolyte, and uncharged and charged states of the systems are shown in the left and right panels, respectively. The EDLC utilizes electrolytes at high ion concentrations (often above 1 M), so that the concentration of the electrolyte between electrodes and in electrode pores does not significantly change upon EDL charging. In contrast, CDI cells are designed to reduce the electrolyte concentration significantly.

easily reclaimed upon discharge of the EDLs without requiring extensive infrastructure.[100–102] To date, CDI has been successfully applied to the desalination of lower salinity (brackish) water streams that typically contain 1000 ppm of total dissolved salts (TDS) (for comparison, seawater is about 35 000 ppm TDS).[101–103] In addition to brackish water desalination, CDI has been used in other applications requiring deionization, such as the treatment of wastewater or purification of power plant boiler water.[101,104]

The feasibility of CDI as a technology for inexpensive, large scale water desalination strongly depends on the availability of electrode materials that are inexpensive, mass producible, foul resistant, environmentally friendly, and whose pore size distribution and surface chemistry can be tuned to fit the requirements of optimized CDI cells. CDI systems developed in the 1960's to early 1990's for water desalination utilized porous carbon-based electrode materials such as activated carbons.[100,105–107] The first CDI system that used CA electrodes was developed in the 1990s by Farmer *et al.* at LLNL.[101,108] CAs offer several advantages over activated carbons, including: (1) a monolithic structure for higher solid phase conductivity, (2) excellent tunability of the pores size distribution (macropores for mass transport, micropores for surface area), (3) the absence of polymeric binders (increasing the chemical stability), and (4) higher specific surface area (>1000 m^2 g^{-1}) thus increasing the ion storage capacity.[101,109] Based on the success of the systems developed at LLNL, CAs subsequently became one of the most common materials used in CDI systems.[100]

Further improvements to CDI electrodes that are needed include (1) reducing the energy required for desalination, (2) optimization of the cell charging/discharging kinetics, and (3) development of desalination of higher ionic strength streams such as seawater. The energy efficiency of a CDI system strongly

depends on the transport losses of both ionic and electric charges. The energy stored in the EDL itself is recoverable upon discharge of the CDI cell. Factors that contribute to the total system resistance include the electric resistance of the solid electrode and the ionic resistance of the salt water in electrode pores and between electrodes. CAs are very conductive due to their monolithic structure, and can reach conductivities up to about 100 S m^{-1} which is over an order of magnitude higher than other porous carbon structures.[28] That is also over one order of magnitude higher than the conductivity of seawater, which is about 5 S m^{-1}, so that the total system resistance becomes dominated by ionic resistance. The highly tunable pore structure of CAs allows for electrode designs that minimize in-pore electrolyte resistance. For example, in a porous medium of a given porosity, decreasing pore size enables a higher surface area to volume ratio, but also higher ionic resistance. By carefully tuning pore size, or by utilization of hierarchically structured CAs with both macro- and micropores,[40] minimization of resistance can be attained while still maintaining ultra-high specific surface area.

3.4 Catalysis

Another promising energy application of CAs related to a hydrogen economy is their use as electrode materials and catalyst support in proton-exchange membrane (PEM) fuel cells. For this application, the electrode needs to combine high electrochemical conductivity, high surface area, and a pore structure that allows for good contact between the catalytically active supported metal nanoparticles, the polymer electrolyte, and the gas phase to minimize mass-transport losses.[110] The advantage of CAs over other more traditional carbon supports such as commercial carbon blacks is that their surface area, pore size and pore volume can be tailored independently from each other.[111] They also offer superior electrical conductivity due to their 3D morphology which reduces the electric losses in the electrode, and they are available as monolithic structures. The required catalytic activity is introduced by metal loading of the otherwise inert CA, and an example of such a CA/metal nanocomposite material is shown in Fig. 11.

The synthesis of CA-supported platinum catalysts and their pore size dependent performance have recently been studied by several groups, and different pore size dependencies have been reported.[26,111–115] For example, Smirnova *et al.*[112] reported a significant increase in cell performance and maximum power density by increasing the average pore size of the CA support from 16 to 20 nm. This result has been attributed to a better penetration of the polymer electrolyte Nafion into larger pores thus enabling a better contact with the Pt nanoparticles distributed on the inner surfaces of the CA support. On the other hand, Marie *et al.*[111] reported that oxygen mass-transport related voltage losses in the cathode layer increase with increasing pore size of the CA support. This result was explained by the observation that Nafion penetration lowers the effective porosity of the CA support thus hindering oxygen mass-transport and that this effect becomes more important with increasing pore size. Clearly, more work on the pore size dependencies of CA-supported fuel cell electrodes is necessary to take full advantage of this novel catalyst material for PEM fuel cell applications. Nevertheless, the results were already very promising.

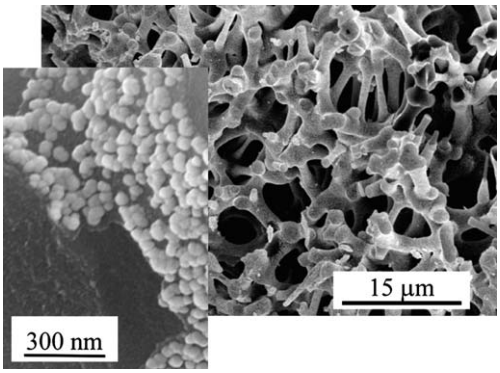

Fig. 11 SEM micrographs of a Ru-loaded CA at different magnification levels. The Ru nanoparticles were deposited using the bis(cyclopentadienyl)ruthenium/air atomic layer deposition processes.

A related technology that also benefits from the tunable mesoporosity of CAs is the biofuel cell[116] that utilizes enzymes or microorganisms adsorbed on the electrode surface to catalyze electro-enzymatic reactions. Here the cell performance should strongly depend on the pore size distribution as the pores need to be large enough to accommodate the large (>10 nm) biomolecules. A dramatic increase of the cell performance with increasing pore size of the CA electrode has indeed been experimentally observed for the electrochemical oxidation reaction of fructose by D-fructose dehydrogenase.[117] As described in previous chapters, the pore size distribution of CAs can easily be tuned by both sol–gel conditions and post-synthesis treatments such as the CO_2 activation what widens preexisting micropores (see Fig. 4).

The PEM fuel cell electrode application discussed above requires the incorporation of metal nanoparticles into the CA structure to add catalytic activity to the otherwise inert CA. Although the loading of CAs with catalytic active materials seems to be simple in theory, it is difficult in practice due to the high aspect ratio of CAs. Indeed, much of the work on Pt loaded fuel cell electrodes has been devoted to the synthesis of highly dispersed Pt nanoparticles. The key issue is the utilization of the catalyst, specifically in the case of expensive noble metals such as platinum or platinum alloys which requires that the catalytically active metal is highly dispersed to maximize its surface area. Furthermore, the metal particles need to be resistant against sintering and stably anchored to the carbon support. Traditionally, metal-loaded CAs have been synthesized by solution impregnation using a suitable metal salt, either during the synthesis of the polymer gel[26] or at a later stage by impregnation of the pyrolized CA.[26,111,113] However, both approaches have their limitations: the former can interfere with the sol–gel process, or can lead to poisoning of the catalyst, for example by coating the Pt nanoparticles with a passivating carbon layer.[26] Loading the final CA structure with metal nanoparticles is difficult because of its high aspect ratio that often involves time intensive and/or complicated steps such as supercritical deposition of metal nanoparticles. Consequently the development of alternative methods has been the subject of many studies.

Vacuum thin film techniques that are commonly used to deposit thin catalyst layers directly onto the membrane or the gas diffusion layer of PEM fuel cells[118] cannot take advantage of the high aspect ratio/mesoporosity of CAs as they are only able to

coat the outer surface. Nevertheless, magnetron sputtering has been used to deposit Pt on thin CA sheets.[114,115] A similar restriction applies to CVD techniques that can be successfully applied to macro-cellular foams,[119] but typically result in inhomogeneous or incomplete coatings on micro–mesoporous substrates.

In the following we will focus on a relatively new approach based on atomic layer deposition (ALD) that has already been successfully used to deposit Pt nanoparticles on solid oxide[120] and PEM[121] fuels cell electrodes. This technique is like no other method suited to deposit material onto the internal surfaces of ultra-high aspect ratio materials such as CAs. ALD is a special variant of the chemical vapor deposition technique that uses a suitable pair of sequential, self-limiting surface reactions (Fig. 12).[122] The technique does not affect the morphology of the aerogel template and offers excellent control over metal loading by simply adjusting the number of ALD cycles. Continuous layers as well as nanoparticles can be grown, depending on the actual surface chemistry. Both oxidic and metallic films and nanoparticles can be deposited, and the technique has been successfully employed to deposit a variety of materials including W,[123] Ru,[52] Pt,[1] Cu,[124] TiO_2[125] and ZnO[126] on various aerogel templates. The two most important metals for the fuel cell application, Pt and Ru, can be deposited following the ALD recipes developed by Aaltonen *et al.*,[127,128] and a typical example is shown in Fig. 13. As both processes run in the same temperature window they also can be combined to deposit Pt–Ru alloy nanoparticles.

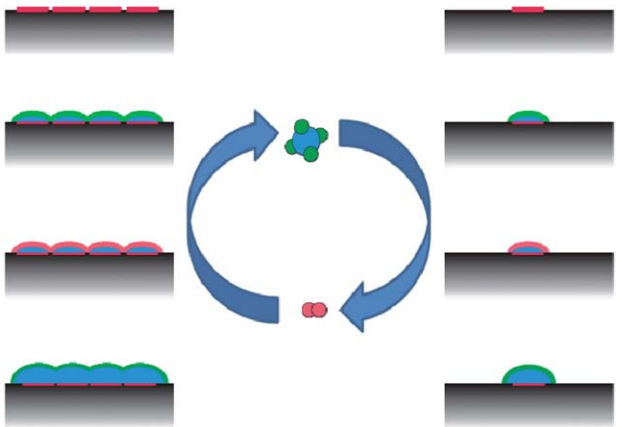

Fig. 12 ALD employs sequential, self-limiting surface reactions to overcome diffusion limitations in high-aspect ratio materials. The underlying principle is that the adsorption of the metal containing precursor poisons the surface thus preventing further precursor uptake (green surface termination), and that the reactive surface state can be regenerated by exposure to the second reactant (red in this example). Both conformal films (left) and individual nanoparticles (right) can be grown, depending on the initial nucleation density which can be influenced by surface treatments.

The catalytic activity of ALD prepared Pt-loaded CAs was tested using the catalytic oxidation of CO with molecular oxygen as a test reaction.[1] The material was catalytically very active with conversion efficiencies of nearly 100%, even at extremely low loading levels (as low as 0.047 mg Pt cm^{-2}).[1] The maximum catalytic activity was reached at only two cycles of ALD. In fact, the catalytic activity was so high that the maximum conversion rate was only limited by the heat produced by the exothermic CO oxidation which increases the temperature of the catalyst to the point where the CA support is attacked by oxygen. This was only observed for very high conversion rates ($\sim 5 \times 10^{-4}$ mol s^{-1} g^{-1}) corresponding to a power production of about 160 W g^{-1}. The high catalytic activity can be attributed to the high dispersion of Pt on the CA surface, and even for the highest loading levels studied (10 ALD cycles), the Pt particle size stayed well below 5 nm (Fig. 13).

4. Summary

CAs hold great technological promise for a variety of sustainable energy applications, including hydrogen and energy storage, desalination, and electrocatalysis. Compared to other porous carbon materials, CAs offer the advantage of a tunable three-dimensional hierarchical morphology and the fact that they are available as macroscopic, centimetre-sized monolithic materials. Combining the morphological diversity of CAs with surface funtionalization can be used to design materials with improved storage capacity and loading/unloading dynamics. To guide the design of these next generation CAs it will be necessary to gain a better understanding of the effect of morphology and surface chemistry on properties such as hydrogen and electrical energy storage capacity. So far, most of the efforts have been focused on increasing the surface area. Further optimization of the storage density will require the synthesis of high-density, high-surface-area CAs. Other promising future research directions include the effect of crystallinity on the properties of CAs, and the effect of space-

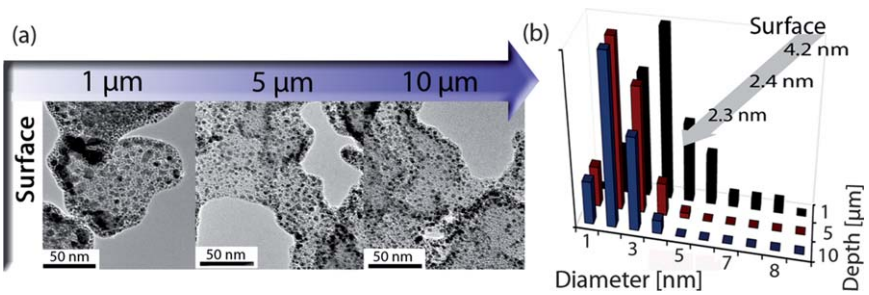

Fig. 13 Morphology of a Pt loaded CA using the (methylcyclopentadienyl)trimethylplatinum (MeCpPtMe3)/oxygen ALD process (10 ALD cycles). (a) Cross-sectional TEM micrographs revealing the high dispersion of Pt. The images were taken at different depths below the outer surface. (b) Corresponding particle size histogram and averaged particle diameters.[1]

charge layer formation on the electronic structure and physical properties of CAs. The importance of the latter effect is, for example, demonstrated by the recent discovery that CA electrodes respond with pronounced length changes upon space-charge layer formation.[129] Here, *in situ* spectroscopic studies will provide the required new insight. Beyond being functional materials by themselves, CAs are also very promising scaffold materials due to their chemical stability that can be used to stabilize other nanomaterials by confinement. These CA-stabilized nanomaterials thus combine the faster kinetics of nanomaterials with the stability of CAs. One specifically promising method to deposit nanomaterials on the inner surfaces of CAs is atomic layer deposition, specifically if the incorporated material is expensive and high utilization is required.

Acknowledgements

Work at LLNL was performed under the auspices of the US DOE by LLNL under Contract DE-AC52-07NA27344 and funded in part by the DOE Office of Energy Efficiency and Renewable Energy. The desalination work was funded in part by the State of California's Proposition 50, funds are administered by the Department of Water Resources.

References

1 J. S. King, A. Wittstock, J. Biener, S. O. Kucheyev, Y. M. Wang, T. F. Baumann, S. K. Giri, A. V. Hamza, M. Bäumer and S. F. Bent, *Nano Lett.*, 2008, **8**, 2405–2409.
2 A. Stein, Z. Wang and M. A. Fierke, *Adv. Mater.*, 2009, **21**, 265–293.
3 Y. S. Hu, P. Adelhelm, B. Smarsly, S. Hore, M. Antonietti and J. Maier, *Adv. Funct. Mater.*, 2007, **17**, 1873–1878.
4 J. Chmiola, G. Yushin, Y. Gogotsi, C. Portet, P. Simon and P. L. Taberna, *Science*, 2006, **313**, 1760–1763.
5 S. Tabata, H. Iida, T. Horie and S. Yamada, *Med. Chem. Commun.*, 2010, **1**, 136–138.
6 K. Lee, J. Lytle, N. Ergang, S. Oh and A. Stein, *Adv. Funct. Mater.*, 2005, **15**, 547–556.
7 G. Chai, I. Shin and J. S. Yu, *Adv. Mater.*, 2004, **16**, 2057–2061.
8 J. Fricke and R. Petricevic, in *Handbook of Porous Solids*, ed. F. Schüth, K. S. W. Sing and J. Weitkamp, Wiley-VCH, Weinheim, 2002.
9 S. S. Kistler, *Nature*, 1931, **127**, 741–741.
10 R. W. Pekala, *J. Mater. Sci.*, 1989, **24**, 3221–3227.
11 R. W. Pekala, *US Pat.*, 4873218, 1989.
12 S. T. Mayer, R. W. Pekala and J. L. Kaschmitter, *J. Electrochem. Soc.*, 1993, **140**, 446–451.
13 T. K. Nielsen, U. Bösenberg, R. Gosalawit, M. Dornheim, Y. Cerenius, F. Besenbacher and T. R. Jensen, *ACS Nano*, 2009, **4**, 3903–3908.
14 G.-R. Li, Z.-P. Feng, Y.-N. Ou, D. Wu, R. Fu and Y.-X. Tong, *Langmuir*, 2010, **26**, 2209–2213.
15 D. R. Rolison, J. W. Long, J. C. Lytle, A. E. Fischer, C. P. Rhodes, T. M. McEvoy, M. E. Bourg and A. M. Lubers, *Chem. Soc. Rev.*, 2009, **38**, 226–252.
16 H. Y. Tian, C. E. Buckley, S. B. Wang and M. F. Zhou, *Carbon*, 2009, **47**, 2128–2130.
17 A. F. Gross, J. J. Vajo, S. L. Van Atta and G. L. Olson, *J. Phys. Chem. C*, 2008, **112**, 5651–5657.
18 A. Feaver, S. Sepehri, P. Shamberger, A. Stowe, T. Autrey and G. Cao, *J. Phys. Chem. B*, 2007, **111**, 7469–7472.
19 H. D. Du, B. H. Li, F. Y. Kang, R. W. Fu and Y. Q. Zeng, *Carbon*, 2007, **45**, 429–435.
20 H. Kabbour, T. F. Baumann, J. H. Satcher, A. Saulnier and C. C. Ahn, *Chem. Mater.*, 2006, **18**, 6085–6087.
21 S. A. Al-Muhtaseb and J. A. Ritter, *Adv. Mater.*, 2003, **15**, 101–114.
22 X. P. Lu, O. Nilsson, J. Fricke and R. W. Pekala, *J. Appl. Phys.*, 1993, **73**, 581–584.
23 S. A. Steiner, T. F. Baumann, J. Kong, J. H. Satcher and M. S. Dresselhaus, *Langmuir*, 2007, **23**, 5161–5166.
24 R. W. Fu, T. F. Baumann, S. Cronin, G. Dresselhaus, M. S. Dresselhaus and J. H. Satcher, *Langmuir*, 2005, **21**, 2647–2651.
25 W. S. Baker, J. W. Long, R. M. Stroud and D. R. Rolison, *J. Non-Cryst. Solids*, 2004, **350**, 80–87.
26 J. Marie, S. Berthon-Fabry, P. Achard, M. Chatenet, A. Pradourat and E. Chainet, *J. Non-Cryst. Solids*, 2004, **350**, 88–96.
27 T. F. Baumann, G. A. Fox, J. H. Satcher, N. Yoshizawa, R. W. Fu and M. S. Dresselhaus, *Langmuir*, 2002, **18**, 7073–7076.
28 M. A. Worsley, P. J. Pauzauskie, T. Y. Olson, J. Biener, J. H. Satcher and T. F. Baumann, *J. Am. Chem. Soc.*, 2010, **132**, 14067–14069.
29 M. A. Worsley, S. O. Kucheyev, J. H. Satcher, A. V. Hamza and T. F. Baumann, *Appl. Phys. Lett.*, 2009, **94**, 073115.
30 M. A. Worsley, P. J. Pauzauskie, S. O. Kucheyev, J. M. Zaug, A. V. Hamza, J. H. Satcher and T. F. Baumann, *Acta Mater.*, 2009, **57**, 5131–5136.
31 M. A. Worsley, J. H. Satcher and T. F. Baumann, *J. Appl. Phys.*, 2009, **105**, 084316.
32 M. A. Worsley, J. H. Satcher and T. F. Baumann, *Langmuir*, 2008, **24**, 9763–9766.
33 T. Bordjiba, M. Mohamedi and L. H. Dao, *J. Power Sources*, 2007, **172**, 991–998.
34 Y. Tao, D. Noguchi, C.-M. Yang, H. Kanoh, H. Tanaka, M. Yudasaka, S. Iijima and K. Kaneko, *Langmuir*, 2007, **23**, 9155–9157.
35 M. A. Worsley, J. H. Satcher and T. F. Baumann, *J. Non-Cryst. Solids*, 2010, **356**, 172–174.
36 A. F. Gross and A. P. Nowak, *Langmuir*, 2010, **26**, 11378–11383.
37 A. H. Lu, B. Spliethoff and F. Schuth, *Chem. Mater.*, 2008, **20**, 5314–5319.
38 T. F. Baumann and J. H. Satcher, *J. Non-Cryst. Solids*, 2004, **350**, 120–125.
39 T. F. Baumann and J. H. Satcher, *Chem. Mater.*, 2003, **15**, 3745–3747.
40 T. F. Baumann, M. A. Worsley, T. Y. J. Han and J. H. Satcher, *J. Non-Cryst. Solids*, 2008, **354**, 3513–3515.
41 A. Feaver and G. Z. Cao, *Carbon*, 2006, **44**, 590–593.
42 C. Lin and J. A. Ritter, *Carbon*, 2000, **38**, 849–861.
43 R. Saliger, U. Fischer, C. Herta and J. Fricke, *J. Non-Cryst. Solids*, 1998, **225**, 81–85.
44 Y. Hanzawa, K. Kaneko, R. W. Pekala and M. S. Dresselhaus, *Langmuir*, 1996, **12**, 6167–6169.
45 M. B. Sassin, A. N. Mansour, K. A. Pettigrew, D. R. Rolison and J. W. Long, *ACS Nano*, 2010, **4**, 4505–4514.
46 J. W. Long, M. B. Sassin, A. E. Fischer, D. R. Rolison, A. N. Mansour, V. S. Johnson, P. E. Stallworth and S. G. Greenbaum, *J. Phys. Chem. C*, 2009, **113**, 17595–17598.
47 A. E. Fischer, M. P. Saunders, K. A. Pettigrew, D. R. Rolison and J. W. Long, *J. Electrochem. Soc.*, 2008, **155**, A246–A252.
48 A. E. Fischer, K. A. Pettigrew, D. R. Rolison, R. M. Stroud and J. W. Long, *Nano Lett.*, 2007, **7**, 281–286.
49 M. A. Worsley, J. D. Kuntz, J. H. Satcher and T. F. Baumann, *J. Mater. Chem.*, 2010, **20**, 4840–4844.
50 M. A. Worsley, J. D. Kuntz, P. J. Pauzauskie, O. Cervantes, J. M. Zaug, A. E. Gash, J. H. Satcher and T. F. Baumann, *J. Mater. Chem.*, 2009, **19**, 5503–5506.
51 M. A. Worsley, J. D. Kuntz, O. Cervantes, T. Y. J. Han, A. E. Gash, J. H. Satcher and T. F. Baumann, *J. Mater. Chem.*, 2009, **19**, 7146–7150.
52 J. Biener, T. F. Baumann, Y. M. Wang, E. J. Nelson, S. O. Kucheyev, A. V. Hamza, M. Kemell, M. Ritala and M. Leskela, *Nanotechnology*, 2007, **18**, 055303.
53 J. W. Elam, J. A. Libera, M. J. Pellin, A. V. Zinovev, J. P. Greene and J. A. Nolen, *Appl. Phys. Lett.*, 2006, **89**, 053124.
54 M. A. Worsley, M. Stadermann, Y. M. Wang, J. H. Satcher and T. F. Baumann, *Chem. Commun.*, 2010, **46**, 9253–9255.
55 T. P. McNicholas, A. M. Wang, K. O'Neill, R. J. Anderson, N. P. Stadie, A. Kleinhammes, P. Parilla, L. Simpson, C. C. Ahn, Y. Q. Wang, Y. Wu and J. Liu, *J. Phys. Chem. C*, 2010, **114**, 13902–13908.
56 C. Guan, K. Wang, C. Yang and X. S. Zhao, *Microporous Mesoporous Mater.*, 2009, **118**, 503–507.
57 K. S. Xia, Q. M. Gao, C. D. Wu, S. Q. Song and M. L. Ruan, *Carbon*, 2007, **45**, 1989–1996.

58 Z. X. Yang, Y. D. Xia and R. Mokaya, *J. Am. Chem. Soc.*, 2007, **129**, 1673–1679.
59 B. Panella, M. Hirscher and S. Roth, *Carbon*, 2005, **43**, 2209–2214.
60 L. Schlapbach and A. Züttel, *Nature*, 2001, **414**, 353–358.
61 K. Denbigh, *The Principles of Chemical Equilibrium*, Cambridge University Press, 1971.
62 R. Chahine and P. Benard, in *Advances in Cryogenic Engineering*, ed. P. Kittel, Plenum Press, New York, 1998, vol. 43, p. 1257.
63 S. Patchkovskii, J. S. Tse, S. N. Yurchenko, L. Zhechkov, T. Heine and G. Seifert, *Proc. Natl. Acad. Sci. U. S. A.*, 2005, **102**, 10439–10444.
64 K. Murata, K. Kaneko, H. Kanoh, D. Kasuya, K. Takahashi, F. Kokai, M. Yudasaka and S. Iijima, *J. Phys. Chem. B*, 2002, **106**, 11132–11138.
65 S. K. Bhatia and A. L. Myers, *Langmuir*, 2006, **22**, 1688–1700.
66 N. P. Stadie, J. J. Purewal, C. C. Ahn and B. Fultz, *Langmuir*, 2010, **26**, 15481–15485.
67 Y. W. Li and R. T. Yang, *J. Phys. Chem. C*, 2007, **111**, 11086–11094.
68 E. Yoo, L. Gao, T. Komatsu, N. Yagai, K. Arai, T. Yamazaki, K. Matsuishi, T. Matsumoto and J. Nakamura, *J. Phys. Chem. B*, 2004, **108**, 18903–18907.
69 A. J. Robell, E. V. Ballou and M. Boudart, *J. Phys. Chem.*, 1964, **68**, 2748–2753.
70 Z. Jin, Z. Sun, L. J. Simpson, K. J. O'Neill, P. A. Parilla, Y. Li, N. P. Stadie, C. C. Ahn, C. Kittrell and J. M. Tour, *J. Am. Chem. Soc.*, 2010, **132**, 15246–15251.
71 Y. H. Kim, Y. F. Zhao, A. Williamson, M. J. Heben and S. B. Zhang, *Phys. Rev. Lett.*, 2006, **96**, 016102.
72 S. I. Orimo, Y. Nakamori, J. R. Eliseo, A. Züttel and C. M. Jensen, *Chem. Rev.*, 2007, **107**, 4111–4132.
73 A. Züttel, P. Wenger, S. Rentsch, P. Sudan, P. Mauron and C. Emmenegger, *J. Power Sources*, 2003, **118**, 1–7.
74 P. E. deJongh, R. W. P. Wagemans, T. M. Eggenhuisen, B. S. Dauvillier, P. B. Radstake, J. D. Meeldijk, J. W. Geus and K. P. de Jong, *Chem. Mater.*, 2007, **19**, 6052–6057.
75 S. Y. Zheng, F. Fang, G. Y. Zhou, G. R. Chen, L. Z. Ouyang, M. Zhu and D. L. Sun, *Chem. Mater.*, 2008, **20**, 3954–3958.
76 C. P. Balde, B. P. C. Hereijgers, J. H. Bitter and K. P. de Jong, *Angew. Chem., Int. Ed.*, 2006, **45**, 3501–3503.
77 A. Gutowska, L. Y. Li, Y. S. Shin, C. M. M. Wang, X. H. S. Li, J. C. Linehan, R. S. Smith, B. D. Kay, B. Schmid, W. Shaw, M. Gutowski and T. Autrey, *Angew. Chem., Int. Ed.*, 2005, **44**, 3578–3582.
78 L. K. Heung and C. G. Wicks, *J. Alloys Compd.*, 1999, **293**, 446–451.
79 R. D. Stephens, A. F. Gross, S. L. Van Atta, J. J. Vajo and F. E. Pinkerton, *Nanotechnology*, 2009, **20**, 204018.
80 WO2005014469, 2003.
81 T. K. Nielsen, K. Manickam, M. Hirscher, F. Besenbacher and T. R. Jensen, *ACS Nano*, 2009, **3**, 3521–3528.
82 S. Zhang, A. F. Gross, S. L. Van Atta, M. Lopez, P. Liu, C. C. Ahn, J. J. Vajo and C. M. Jensen, *Nanotechnology*, 2009, **20**, 204027.
83 R. Bogerd, P. Adelhelm, J. H. Meeldijk, K. P. de Jong and P. E. de Jongh, *Nanotechnology*, 2009, **20**, 204019.
84 A. F. Gross, C. C. Ahn, S. L. Van Atta, P. Liu and J. J. Vajo, *Nanotechnology*, 2009, **20**, 204005.
85 S. Sepehri, A. Feaver, W. J. Shaw, C. J. Howard, Q. Zhang, T. Autrey and G. Cao, *J. Phys. Chem. B*, 2007, **111**, 14285–14289.
86 R. W. Pekala, J. C. Farmer, C. T. Alviso, T. D. Tran, S. T. Mayer, J. M. Miller and B. Dunn, *J. Non-Cryst. Solids*, 1998, **225**, 74–80.
87 B. E. Conway, *J. Electrochem. Soc.*, 1991, **138**, 1539–1548.
88 BES Workshop, *Technology and Applied R&D Needs for Electrical Energy Storage*, 2007.
89 J. Gamby, P. L. Taberna, P. Simon, J. F. Fauvarque and M. Chesneau, *J. Power Sources*, 2001, **101**, 109–116.
90 D. B. Robinson, *J. Power Sources*, 195, 3748–3756.
91 J.-P. Randin and E. Yeager, *J. Electroanal. Chem. Interfacial Electrochem.*, 1972, **36**, 257–276.
92 E. Frackowiak and F. Béguin, *Carbon*, 2001, **39**, 937–950.
93 S.-W. Woo, K. Dokko and K. Kanamura, *J. Power Sources*, 2008, **185**, 1589–1593.
94 J. S. Sakamoto and B. Dunn, *J. Mater. Chem.*, 2002, **12**, 2859–2861.
95 J. W. Long, B. Dunn, D. R. Rolison and H. S. White, *Chem. Rev.*, 2004, **104**, 4463–4492.
96 L. Bazin, S. Mitra, P. L. Taberna, P. Poizot, M. Gressier, M. J. Menu, A. Barnabé, P. Simon and J. M. Tarascon, *J. Power Sources*, 2009, **188**, 578–582.
97 S. K. Cheah, E. Perre, M. r. Rooth, M. Fondell, A. Hårsta, L. Nyholm, M. Boman, T. r. Gustafsson, J. Lu, P. Simon and K. Edström, *Nano Lett.*, 2009, **9**, 3230–3233.
98 M. A. Shannon, P. W. Bohn, M. Elimelech, J. G. Georgiadis, B. J. Marinas and A. M. Mayes, *Nature*, 2008, **452**, 301–310.
99 National Research Council, *Committee on Advancing Desalination Technology, Desalination: a National Perspective*, National Academies Press, Washington DC, 2008.
100 Y. Oren, *Desalination*, 2008, **228**, 10–29.
101 J. C. Farmer, D. V. Fix, G. V. Mack, R. W. Pekala and J. F. Poco, *J. Electrochem. Soc.*, 1996, **143**, 159–169.
102 C. J. Gabelich, T. D. Tran and I. H. Suffet, *Environ. Sci. Technol.*, 2002, **36**, 3010–3019.
103 P. M. Biesheuvel and A. van der Wal, *J. Membr. Sci.*, 2010, **346**, 256–262.
104 J.-B. Lee, K.-K. Park, H.-M. Eum and C.-W. Lee, *Desalination*, 2006, **196**, 125–134.
105 G. W. Murphy and J. H. Tucker, *Desalination*, 1966, **1**, 247–259.
106 A. M. Johnson and N. John, *J. Electrochem. Soc.*, 1971, **118**, 510–517.
107 Y. Oren and A. Soffer, *J. Appl. Electrochem.*, 1982, **13**, 473–487.
108 J. C. Farmer, D. V. Fix, G. V. Mack, R. W. Pekala and J. F. Poco, *J. Appl. Electrochem.*, 1996, **26**, 1007–1018.
109 J. Wang, L. Angnes, H. Tobias, R. A. Roesner, K. C. Hong, R. S. Glass, F. M. Kong and R. W. Pekala, *Anal. Chem.*, 1993, **65**, 2300–2303.
110 A. L. Dicks, *J. Power Sources*, 2006, **156**, 128–141.
111 J. Marie, R. Chenitz, M. Chatenet, S. Berthon-Fabry, N. Cornet and P. Achard, *J. Power Sources*, 2009, **190**, 423–434.
112 A. Smirnova, X. Dong, H. Hara, A. Vasiliev and N. Sammes, *Int. J. Hydrogen Energy*, 2005, **30**, 149–158.
113 J. Marie, S. Berthon-Fabry, M. Chatenet, E. Chainet, R. Pirard, N. Cornet and P. Achard, *J. Appl. Electrochem.*, 2007, **37**, 147–153.
114 M. Glora, M. Wiener, R. Petricevic, H. Probstle and J. Fricke, *J. Non-Cryst. Solids*, 2001, **285**, 283–287.
115 R. Petricevic, M. Glora and J. Fricke, *Carbon*, 2001, **39**, 857–867.
116 Y. Miura, S. Tsujimura, S. Kurose, Y. Kamitaka, K. Kataoka, T. Sakurai and K. Kano, *Fuel Cells*, 2009, **9**, 70–78.
117 S. Tsujimura, A. Nishina, Y. Hamano, K. Kano and S. Shiraishi, *Electrochem. Commun.*, 2010, **12**, 446–449.
118 S. Litster and G. McLean, *J. Power Sources*, 2004, **130**, 61–76.
119 D. T. Queheillalt, D. D. Hass, D. J. Sypeck and H. N. G. Wadley, *J. Mater. Res.*, 2001, **16**, 1028–1036.
120 X. R. Jiang, H. Huang, F. B. Prinz and S. F. Bent, *Chem. Mater.*, 2008, **20**, 3897–3905.
121 C. Liu, C. C. Wang, C. C. Kei, Y. C. Hsueh and T. P. Perng, *Small*, 2009, **5**, 1535–1538.
122 S. M. George, *Chem. Rev.*, 2010, **110**, 111–131.
123 T. F. Baumann, J. Biener, Y. M. M. Wang, S. O. Kucheyev, E. J. Nelson, J. H. Satcher, J. W. Elam, M. J. Pellin and A. V. Hamza, *Chem. Mater.*, 2006, **18**, 6106–6108.
124 S. O. Kucheyev, J. Biener, T. F. Baumann, Y. M. Wang, A. V. Hamza, Z. Li, D. K. Lee and R. G. Gordon, *Langmuir*, 2008, **24**, 943–948.
125 S. Ghosal, T. F. Baumann, J. S. King, S. O. Kucheyev, Y. M. Wang, M. A. Worsley, J. Biener, S. F. Bent and A. V. Hamza, *Chem. Mater.*, 2009, **21**, 1989–1992.
126 S. O. Kucheyev, J. Biener, Y. M. Wang, T. F. Baumann, K. J. Wu, T. van Buuren, A. V. Hamza, J. H. Satcher, J. W. Elam and M. J. Pellin, *Appl. Phys. Lett.*, 2005, **86**, 083108.
127 T. Aaltonen, M. Ritala, T. Sajavaara, J. Keinonen and M. Leskela, *Chem. Mater.*, 2003, **15**, 1924–1928.
128 T. Aaltonen, P. Alen, M. Ritala and M. Leskela, *Chem. Vap. Deposition*, 2003, **9**, 45–49.
129 L. H. Shao, J. Biener, D. Kramer, R. N. Viswanath, T. F. Baumann, A. V. Hamza and J. Weissmuller, *Phys. Chem. Chem. Phys.*, 12, 7580–7587.